Solar Energy 182 (2019) 480–490

Contents lists available at ScienceDirect

Solar Energy

journal homepage: www.elsevier.com/locate/solener

Solar treatment of cohesive particles in a directly irradiated rotary kiln

Gkiokchan Moumin[a,*], Stefania Tescari[b], Pradeepkumar Sundarraj[b], Lamark de Oliveira[b], Martin Roeb[b], Christian Sattler[b]

[a] German Aerospace Center (DLR), Professor-Rehm-Str. 1, 52428 Juelich, Germany
[b] German Aerospace Center (DLR), Linder Hoehe, 51147 Cologne, Germany

ARTICLE INFO

Keywords:
Solar rotary kiln
Solar calcination
Cement production
Lime production
Limestone
Cohesive

ABSTRACT

Although the utilization of concentrated solar power (CSP) for electricity production is already at commercial stage, the application to energy intensive industrial processes is still at an early stage. Among these, the cement industry is one of the biggest CO_2-emitters and requires temperature levels achievable with concentrated solar radiation. Since fine particles have to be treated in this process, several challenges arise from the implementation of solar energy in such applications. In this work we present the design and experimental assessment of a high temperature solar rotary kiln to perform the calcination of cement raw meal. With input powers of about 14 kW, material flows of 4–12 kg/h were treated and calcination degrees ranged from 24 to 99%. The chemical efficiency was between 8 and 20% while total efficiencies (thermal plus chemical) between 19 and 40% were achieved. The creation of dust, which is a major issue with particles in the μm-range, could be kept under control by applying a suitable suction system at the reactor aperture. The influence of the mass flow rate, residence time and kiln temperatures on the calcination were analysed to identify key points for further improvement.

1. Introduction

A global shift from fossil energy towards renewable energy resources is in progress. Concentrated solar power (CSP) technology is rapidly increasing its contribution for electricity generation in sunny regions with 96 plants already in operation (NREL, 2018). The field of heat transfer fluids (HTF) used in CSP technology till date is dominated by liquids. One promising candidate for HTFs are solids in the form of small particles (Falcone et al., 1985). In general, particles can be separated in granules and powders (Andreotti et al., 2013). The difference is that granules have a size bigger than 100 μm whereas powders have particle diameters between 1 and 100 μm (Andreotti et al., 2013). Granules do not show any cohesive behaviour and hence the handling becomes much easier because of their superior flowability, constant angle of repose, and non-compressibility, when compared to powders (Lumay et al., 2012). The research in the area of electricity production via CSP is therefore focused on granules (Ho, 2016), such as sintered bauxite. Reactors treating particles were also proposed for different chemical applications. Except for volatile materials (which experience a solid-gas phase change during the chemical process) and fixed bed reactors, the work on cohesive particles is very limited (Alonso and Romero, 2015).

Powders are however required in processes in which chemical reactions take place and a high homogeneity of the mixture is needed. An example for this is the cement production (Kohlhaas and Labahn, 1983), which is responsible for 8% of the human-caused CO_2 emissions (Olivier et al., 2016) and half of these emissions are produced by combustion. The production is split into two successive thermal steps: the calcination at 900 °C and the sintering at 1350–1500 °C (Sprung, 2008). During the sintering new phases are formed through chemical reactions, requiring a high homogeneity of the bed and thus needing a finely ground powder (Kohlhaas and Labahn, 1983). The material is ground before the thermal treatments begin. A grinding after the calcination would require the cooling of the material to avoid damage to the grinding rolls. Most of the energy for the thermal treatment is consumed for the calcination of the cement raw meal (CRM) which is a mixture of limestone (about 80%), clay and sand. In a typical cement plant, up to 65% of the fuel is consumed by the calcination (Sprung, 2008), which is described as follows (Oates, 1998):

$$CaCO_3(s) \rightarrow CaO(s) + CO_2(g),\ \Delta H_R = 178.3\ \frac{kJ}{mol}\ \text{at } 25\ °C. \quad (1)$$

This reaction starts at temperatures above 700 °C in air, and 900 °C in pure CO_2 atmosphere (Oates, 1998). Particle treatment in this temperature range is feasible using existing CSP technology (Ho, 2016; Alonso and Romero, 2015).

The solar calcination of limestone has been experimentally analysed in several previous studies, as summarized in Table 1. Generally, three

* Corresponding author.

https://doi.org/10.1016/j.solener.2019.01.093
Received 1 October 2018; Received in revised form 25 January 2019; Accepted 28 January 2019

types of efficiencies are defined to characterize the reactors. The thermal efficiency η_{th} is defined as the ratio of sensible heat taken by the material to the incoming heat flux. The chemical efficiency η_{ch} is defined as the ratio of energy consumed by the reaction to the incoming heat flux. For this calculation the degree of calcination X_{calc} is also considered. The total efficiency η_{tot} is the sum of the thermal and chemical efficiency.

The first trials on solar calcination were made in 1980 by Flamant et al. in two different directly irradiated reactors, a fluidized bed and a rotary kiln (Flamant et al., 1980). In the fluidized bed reactor the particles were in a controlled atmosphere (closed reactor), whereas in the rotary kiln the particles were in contact with ambient air (open reactor). The size of the particles utilized ranged between 200 and 315 μm. The total efficiency, considering the heating and the reaction, was in the range of 10–20% for the fluidized bed with calcination degrees from 80 to 100%. In the rotary kiln total efficiencies were 7–15% for calcination degrees from 30 to 60%.

Further research was carried out by Meier et al. in 2004 and 2005 using a solar rotary kiln in an open and a closed configuration (Meier et al., 2004, 2005, 2006). The calcination of limestone particles in the size of 1–5 mm was performed. In the open configuration the particles are directly irradiated, whereas in the closed configuration an intermediate surface (recrystallized SiC tubes) is used to transfer the heat from solar radiation to the particles (indirect heating). The concept was based on a multi-tube configuration, in which the particles are fed through 16 absorber tubes arranged concentrically inside the rotating cavity. The reason stated for moving from the open to the closed configuration is the severity of dust formation in the open configuration (Meier et al., 2006). The dust formation has two main impacts on the operation of the kiln. First, additional effort is needed to avoid the uncontrolled emission of particles to the environment. Second, the dust cloud attenuates a significant part of the incident radiation. The influence of the cloud was not further analysed (Meier et al., 2006). Experimental results with the closed reactor showed high calcination degrees above 98% and high chemical efficiencies of up to 35%. The use of such a reactor with fine and cohesive particles would be difficult to realize due to the adhesion of particles on the inner surface of the heated tubes.

The most recent experimental work on the calcination of limestone was performed by Tregambi et al. in 2018. The work is not limited to the calcination of the material but treats the complete calcination-recarbonation cycle, the so-called calcium looping (Tregambi et al., 2018a). Calcium looping is considered as a possibility for capturing CO_2 from flue gasses during the recarbonation and a subsequent controlled release of the CO_2 during the calcination. The fluidized bed reactor was fed batch-wise with $CaCO_3$-particles in a size range of 420–590 μm. Four cycles of calcination and carbonation were performed, showing decreasing capture efficiency. The cause for this was given as the sintering of the particles since lower overall specific pore volumes were measured after the third calcination step. In a later publication, 120 g of lime was produced for the use in the cement production and the quality of this cement was assessed (Tregambi et al., 2018b). Portland cement samples produced with conventional lime and solar produced lime were compared in regard to their lime saturation factor, burnability, phase composition and hydration behaviour. No significant deviation was found between the compared samples. The studies of Tregambi et al. focussed on the general feasibility of the calcium looping and on the cement quality with solar calcined lime, which is why no efficiencies are given (Tregambi et al., 2018a, 2018b).

Reactors described above dealt with the calcination of granular, non-cohesive particles. This is reasonable if the final product is lime (CaO), but it is not suitable for cement production, where cohesive particles in the form of powder are treated. Studies focussing on the treatment of fine and cohesive limestone or CRM using CSP technology are very limited. Up to now it has been analysed only in three cyclone reactors, of which one was not focussed on the calcination but coproduction of lime, and an indirect rotary tube reactor.

Imhof et al. and Steinfeld et al. studied in 1991 and 1992 the calcination of pure calcium carbonate particles in a size range of 1–5 μm using a directly irradiated open cyclone reactor (Imhof, 1991; Imhof et al., 1991; Steinfeld et al., 1992). The concept is based on the calcination of the particles with the swirling gas stream followed by the separation of the particles from the gas stream. The cyclone was placed horizontally and the product could be collected at the narrow side of the cyclone. A second cyclone separated the remaining fines in the gas stream. The total efficiency reached 43% while calcination degrees of 53–94% were achieved. In later studies, the reactor size was increased and its working principle was changed (Imhof, 1996, 1997, 2000). Cyclone separators are able to collect most of the particles if they are bigger than 10 μm (Rhodes, 2008). By changing the geometry and inserting particles smaller than this threshold, the entrainment of the gas stream was utilized. 99% of the particles were smaller than 10 μm, allowing the extraction of the product with the gas stream. The cyclone was placed vertically and was irradiated from the bottom. The entrainment of the particles was also utilized to avoid any emission through the opening to the environment. Imhof was the first to experimentally analyse the calcination of CRM. The degree of calcination was in the range of 32–85% (Imhof, 2000). A total efficiency of up to 88% was obtained, which includes the heating of the air as useful heat, since it was used in a heat exchanger to preheat the reactants. At the same time the chemical efficiency reached 15%. The difference in thermal and chemical efficiency is due to the fact that the cyclone reactor is operated with an air flow six times higher than the particle flow (Imhof, 2000).

Nikulshina et al. analysed in 2009 the coproduction of syngas and lime by combined limestone calcination and dry reformation of methane using a particle-flow reactor (Nikulshina et al., 2009). The CO_2 emitted during the calcination is taken up by the reformation reaction. The mean particle size of the limestone was 6 μm for all runs. Chemical efficiencies, for the calcination and reforming, varied in the range of 7–10% with conversion rates of 83% and 38% for limestone and methane, respectively. Considering the reaction enthalpies for each reaction, the efficiency for the calcination can be estimated as about 2–4%.

Recently, Abanades and André carried out experimental analysis on an indirectly heated rotary tube to calcine $CaCO_3$-particles (Abanades and André, 2018). The particles were sieved to obtain a particle size in the range of 50–100 μm. The reactor was operated successfully and high calcination degrees up to 100% were achieved. The reactor dimensions were comparatively small and only flow rates up to 163 g/h were treated with a chemical efficiency of 10%. As with the work from Meier et al. in 2006, the issue of adhesion of particles on the inner walls of the pipe is an uncertainty for the upscaling of such a design.

Up to now the solar calcination of powders at relevant scale was shown only in a cyclone reactor. Although high calcination could be achieved, a drawback of such a reactor is the limitation in treatable particle size. Inserting a raw material with a broader particle size range than tested would result in the deposition of the bigger particles in the cyclone or an uncontrolled emission to the environment through the opening. Moreover high air flows to entrain the particles, limits the chemical efficiency of this reactor concept.

In this work we present the successful operation of an open and directly heated solar rotary kiln for the calcination of CRM powder, having a wide particle size distribution. One open and one closed configuration are tested to show the capability and limitation of each configuration. A comparison of both configurations is made to identify the losses and to define the most important aspects for a potential upscaling. The results, detailed in the following sections, are summarized in Table 1.

Table 1
Literature review of solar calcination reactors.

Author	Flamant et al. (1980)		Steinfeld et al. (1992)	Imhof (1996, 1997, 2000)	Meier et al. (2004)	Meier et al., 2006, 2005)	Nikulshina et al. (2009)	Abanades and André (2018)	Tregambi et al. (2018b, 2018a)	This work	
Year	1980		1992	1996	2004	2005	2009	2018	2018	2018	
Reactor type	FB	RK	CY	CY	RK	RK	CY	Rotary tube	FB	RK	
Irradiation	Direct	Direct	Direct	Direct	Direct	Indirect	Direct	Indirect	Direct	Direct	
Open	No	Yes	Yes	Yes	Yes	No	No	No	No	Yes	
Height/Length	300 mm	90 mm	300 mm	800 mm	600 mm	225 mm	210 mm	400 mm	100 mm	735 mm	
Diameter	35 mm	20 mm/ 24 mm	200 mm	540 mm	350 mm	252 mm	120 mm	20 mm	100 mm	240 mm	
Aperture	–	20 mm/ 24 mm	60 mm	170 mm	350 mm	80 mm	50 mm	15 mm	–	130 mm	
Operation	Batch	Cont. / Batch	Cont.	Cont.	Cont.	Cont.	Cont.	Cont.	Batch	Cont.	
Power	1.7 kW	1.5 kW	3 kW	54 kW	10 kW	10.6 kW	3.7 kW	0.75 kW	3.2 kW	14.2 kW	
Particle size	200–315 µm		1–5 µm	< 10 µm	2–3 mm	2–3 mm	6 µm	50–100 µm	420–590 µm	< 176 µm (D50 = 15 µm)	
Mass flow ($CaCO_3$, feed)	10 g	0.28 kg/h/8 g	0.6 kg/h	18.8 kg/h[a]	2.3 kg/h	7 kg/h	0.18 kg/h	0.16 kg/h	120 g	9.6 kg/h[a]	6.2 kg/h[a]
X_{calc}	80%/100%	30%/60%	53–94%	32–85%	> 95%	> 98%	83%	100%	88%[b]	44–73%	> 95%
η_{th}	–	–	34%[b]	73%[b]	–	22%	–	7%[b]	–	22%	17%
η_{ch}	–	–	9%[b]	15%	20%	35%	2–4%[b]	10%[b]	–	15%	20%
η_{tot}	20%/ 10–15%	7%/15%	43%	88%	–	57%	–	17%	–	37%	37%

FB = fluidized bed, RK = rotary kiln, CY = cyclone.
[a] Used material is cement raw meal (CRM). $CaCO_3$ amount determined by own calculation according to composition.
[b] Own calculation according to given data in references.

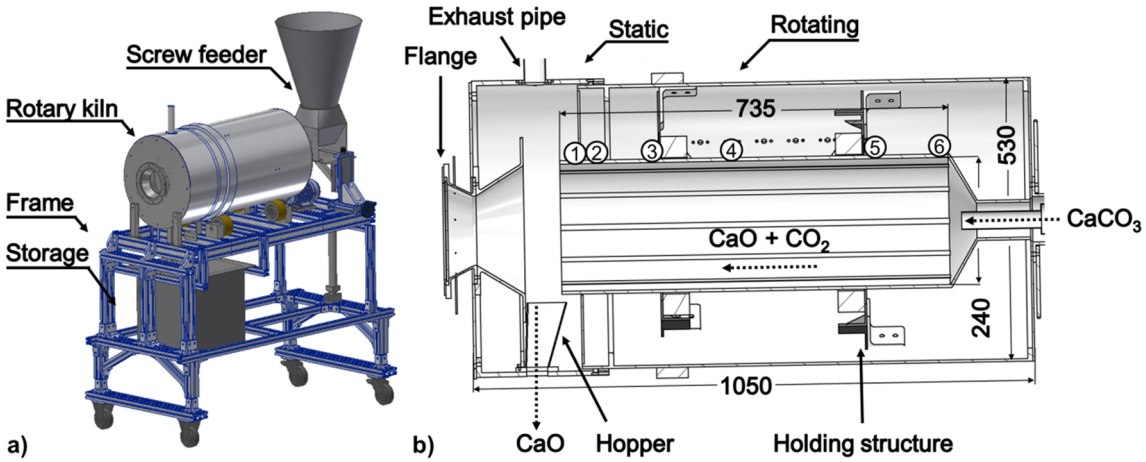

Fig. 1. (a) CAD sketch of the whole system and (b) section view of the rotary kiln indicating the components and the positions of the thermocouples (1–6). The dimensions are given in mm.

2. Experimental setup

The experimental setup employed for the calcination of CRM is shown in Fig. 1a. It consists of four main components: the screw feeder, rotary kiln, storage and frame. The screw feeder is used for feeding the particles into the rotary kiln from the back (see Fig. 1b) at a desired flow rate. The rate is regulated by adjusting the power of the feeder motor. Calibrations were done to obtain the correlations for the different materials. The tube of the screw feeder is water-cooled to reduce the heat transfer from the screw auger to the motor shaft, in order to avoid damage of the motor due to overheating. The outer housing of the kiln is made of aluminium and is 1050 mm in length and 530 mm in diameter. The kiln is placed over four wheels and rotated using a motor through a toothed wheel fixed on the back of the housing. The crucible is made of Inconel 600 and is 735 mm in length, 240 mm in diameter, and 5 mm in thickness.

Particle mixing inside the bed is crucial for rotary kilns. Henein et al. described six types of bed motions and summarized them in a bed behaviour diagram (Henein et al., 1983). The optimal bed mixing is obtained when the particles move in a rolling mode, where constant renewal of the particles at the top layer with those at the bottom layer is achieved (Fig. 2b). A periodical renewal of the layer is defined as the slumping motion. On the contrary, in the slipping motion the particles in the bed do not move relative to each other and no mixing occurs (Fig. 2a).

Cohesive particles which do not flow freely tend to have very low mixing. In order to avoid slippage of the particle bed 12 strips (10 × 1 × 735 mm) are welded inside the crucible surface, as shown in Fig. 2b. The strips induce collapses of the bed during rotation and improve the mixing in the transversal plane. These regular collapses correspond to a slumping or rolling motion is shown in Fig. 2b. The number and shape of the strips was chosen during cold tests by visually comparing different shapes, maximizing the number of collapses and minimizing the dust production.

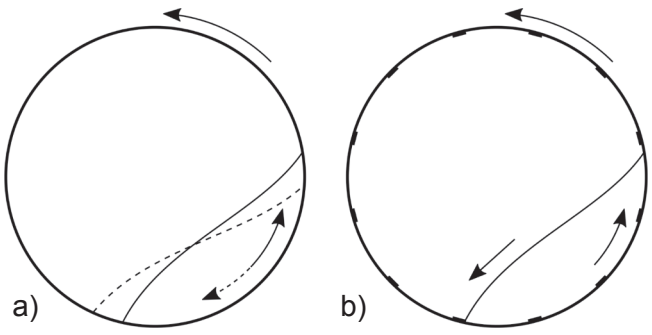

Fig. 2. Visualisation of the bed motion in (a) a smooth crucible, where an oscillating movement of the complete bed takes place (slipping motion) and (b) the crucible in this work with 12 strips welded on the inside, where regular collapses of the bed take place (slumping/rolling motion).

The crucible is fixed in its position axially by the holding structures (1.4828 and 1.4841) connected to the outer aluminium housing (see Fig. 1b). The rotating housing is inserted inside the static front housing, which comprises of the flange, gas exhaust pipe and the hopper at the bottom. At the aperture, through which solar radiation enters, a conical flange (Inconel 600) is mounted to allow the attachment of a window. The reacted particles leave the reactor through the hopper and are collected in the storage. The kiln, feeder and storage are mounted on a frame as shown in Fig. 1a. To allow different angles of inclination, the upper plane of the frame can be inclined through a hydraulic jack. A sealing between the front and the outer housing prevents particles or gas exiting.

The space between crucible and outer housing is insulated with two different ceramic fibre blankets ultrawool 1100 and 650 supplied by the manufacturer elisto GmbH, Germany. Thermal conductivities are correspondingly 0.04 W/m/K at 800 °C and 0.035 W/m/K at 600 °C. The space between the two blanket layers is packed with the ceramic fibre wool SILCAFLEX 126, supplied by silca GmbH, Germany. The wool has a thermal conductivity of 0.25 W/m/K at 1000 °C and allowed the insulation of parts difficult to access. The front housing is insulated with the same material with openings for the flange, gas exhaust pipe and the hopper. Six Type-K thermocouples are inserted through the rotating housing and brought in contact with the outer surface of the crucible to measure its temperature (see Fig. 1b). The thermocouples are referred to as WTC 01–06 and are respectively placed at a distance of 28 mm, 55 mm, 175 mm, 325 mm, 615 mm and 735 mm, from the front of the crucible, respectively. Two more thermocouples are used to measure the outer temperature of the rotating housing. The data measured from the rotating part is transferred through a WiFi-module to the software.

Reactor performances were assessed first through a thermal experimental campaign, in which inert, non-cohesive particles were heated up (Tescari et al., 2017). Afterwards a chemical experimental campaign with cohesive CRM was carried out. During the chemical tests CO_2 evolves from the bed, intensifying the dust formation inside the kiln. Meier et al. (2006) observed in their open configuration reactor a white powder cloud evolving from the bed and exiting the reactor, which attenuates a significant part of the incident power entering the reactor through absorption and reflection. To prevent this, in the present study the gas path through the reactor was controlled through an

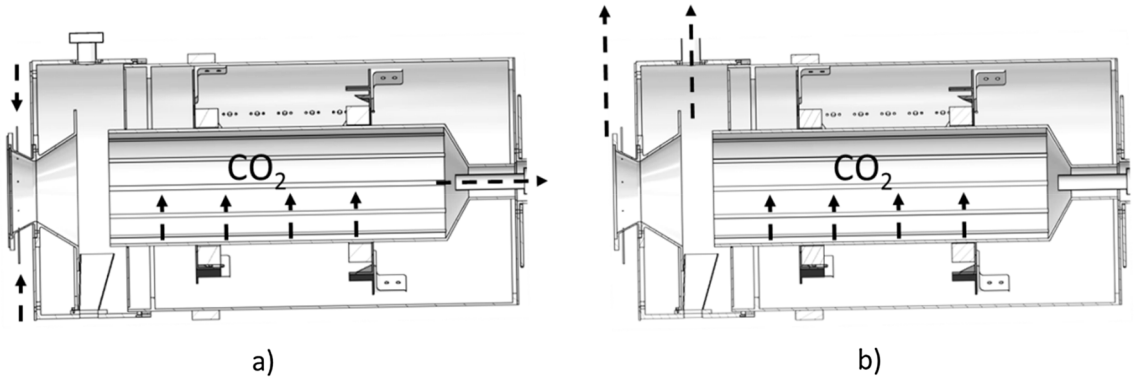

Fig. 3. Visualisation of (a) the closed configuration where purge gas flow can be injected at the window and suction can be applied at the back and (b) the open configuration where suction can be applied before and behind the aperture.

extraction system. In this system, the gas produced by the reaction was extracted by a blower, after passing through a water cooler and a paper filter.

Two different reactor configurations were analysed. First, a closed one with a quartz window covering the aperture was tested. A purge gas flow could be injected radially at the window and suction could be applied at the back (Fig. 3a). The purge gas was compressed air with a maximum flow of 20 l/min (at 20 °C). The gas extraction from the back was realised with four pipes 10 mm in diameter and a maximum suction flow of 100 l/min. In the case of 100% calcination and for a material flow of about 10 kg/h of CRM, a flow rate of CO_2 in the range of 50 l/min was expected (at 20 °C). Second, an open configuration without window and with two suction positions at the reactor front was tested (see Fig. 3b). One of the suctions was applied at the upper exhaust pipe and one above the front flange, providing suction of about 750 l/min each. The extraction point at the front flange was used to prevent contamination of the experimental room. Cold experiments with CRM validated the feasibility of both concepts.

During a typical experiment in the solar simulator, the CRM is heated up and calcined. The low CO_2 concentration present in air when the material cools down prevents significant re-carbonation of the material. The calcination of the treated CRM was quantified through thermogravimetric analysis (Netzsch STA 449 F3 Jupiter). During a TGA test, 100–150 mg of solar calcined CRM was heated up to 1000 °C in Ar-atmosphere and kept at this temperature for 30 min. Empty measurements were subtracted for all experiments to account for baseline drifts. The weight loss after the experiment defined the reaction extent. The weight loss, compared with a reference case where unprocessed CRM is completely calcined, was used to calculate the calcination degree X_{calc} during the solar experiment:

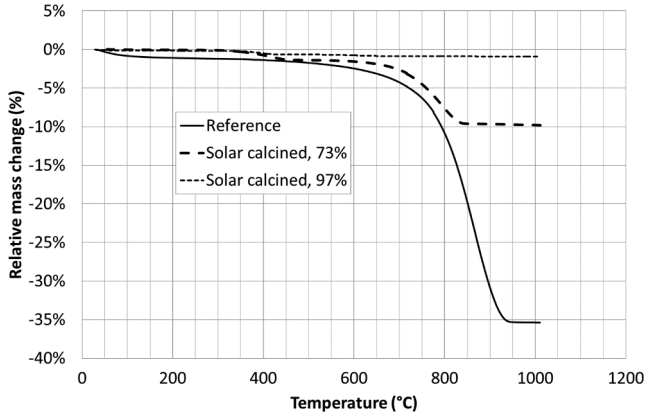

Fig. 4. TGA results for a reference CRM and two solar calcined samples.

$$X_{calc} = 1 - \frac{\Delta m_{sample}}{\Delta m_{reference}} [\%]. \quad (2)$$

The analysis and a comparison with samples are shown in Fig. 4. For each experiment, three samples were collected at different heights of the storage (top, middle and bottom) to monitor the variation of the calcination during the operation. The thermal and chemical efficiencies are defined according to:

$$\eta_{th} = \frac{\dot{Q}_{thermal}}{\dot{Q}_{solar}} = \frac{\dot{m} \cdot c_p \cdot \Delta T}{\dot{Q}_{solar}} \quad \text{and} \quad \eta_{ch} = \frac{\dot{Q}_{chemical}}{\dot{Q}_{solar}} = \frac{\dot{m} \cdot \Delta H_R \cdot X_{calc}}{\dot{Q}_{solar}}, \quad (3)$$

where $\dot{m}$ represents the particle mass flow, c_p is the temperature dependent specific heat, ΔT is the temperature difference between inlet (room temperature) and outlet (WTC 01), $\dot{Q}_{solar}$ is the incoming heat flux at the aperture and ΔH_R is the reaction enthalpy of the calcination at ambient temperature which is 1781 kJ/kg for $CaCO_3$ (Oates, 1998). The enthalpy is adjusted with the $CaCO_3$ content in the CRM which in our case varies between 80 and 84%. Although the chemical reaction, and thus the chemical efficiency is of main interest, the thermal efficiency has also to be considered for a complete assessment of the reactor. In the cement production the calcined material has to be fed to the succeeding sintering process which takes place at 1350–1500 °C. Any thermal losses in the calcination process correspond to a higher fuel consumption in the sintering process. The total efficiency η_{tot} is defined as the sum of the two efficiencies.

For the inert tests bauxite particles with a diameter of 980 µm were used. The CRM samples were provided by the cement manufacturer CEMEX. The particles have a broad particle size distribution in the range of 1–176 µm. However, 90% of the CRM mass is made up of particles smaller than 101 µm, while 50% is smaller than 15 µm. A comparison of the inert and reactive particle properties is given in Table 2.

The tests were carried out in the high flux solar simulator located at the DLR site in Cologne, Germany. The simulator has 10 xenon short-arc lamps which can provide 20 kW of thermal power at the focal plane (Dibowski et al., 2007). During a typical run, the incident power is increased step-wise, starting with 2 lamps and turning on one lamp every 10 min, to limit the thermal stresses. Maximum power input of 15.96 kW at the aperture is achieved. The focal plane is located at the aperture and the corresponding flux map is given in Fig. 5. The radiation diverges after passing the narrowing of the aperture flange and hits mainly the lateral surfaces of the crucible. The inclination of the kiln is set in all experiments to 1° whereas the rotational speed is 2 rpm.

3. Results and discussion

In total, 21 tests were successfully performed with the reactor. Out of those, 4 were done with Bauxite particles and 17 with CRM particles. The results in the closed configuration will be presented first, followed

Table 2
Properties of inert and reactive particles used in the experimental campaigns.

	Bauxite (SG10 16/30 from Saint Gobain)	Cement raw meal
Composition	74 wt% Al_2O_3 26 wt% Fe_2O_3, SiO_2, TiO_2	80–84 wt% $CaCO_3$ 20–26 wt% SiO_2, Al_2O_3, Fe_2O_3
Particle size (μm)	980 (mean) (Saint-Gobain, 2013)	1–176 (D50 = 15, D90 = 101)
Specific heat capacity (J/kg/K)	$9.565 \cdot 10^{-7} \cdot T^3 - 2.913 \cdot 10^{-3} \cdot T^2 + 3.011 \cdot T - 102.9$ (T in K) (adopted from (Wicks and Block, 1963))	$880 + 0.293 \cdot T$ (T in °C) (Kohlhaas and Labahn, 1983)

by those in the open configuration.

3.1. Closed configuration

The closed configuration is initially tested with inert particles. Fig. 6 shows a typical thermal experiment, which lasts 4 h. The purge gas flow during the run is set to 0 l/min whereas the suction is operated at 50 l/min. The suction power was constant during all experiments, and set to the maximum capacity of the blower. Since the reactor is not completely gas tight, air is sucked in from the environment. In the heating phase, the reactor is heated to a temperature of about 1000 °C in 1.25 h. After heating up, the bauxite particles are fed into the reactor at a rate of 28.7 kg/h. The temperatures at the back (particle entrance) drop very rapidly below 600 °C while the centre part (WTC 04) stabilizes at around 840 °C. The crucible temperature reaches a peak of 1090 °C at 55 mm from the front (WTC 02) and then decreases to 1060 °C at 28 mm (WTC 01). The feeding is stopped after 1.5 h followed by a sharp increase in the back temperature (WTC 05 and 06). This sudden temperature variation also allows detecting an eventual flow variation due to malfunctioning of the feeding system or motor. At the same time the incident power is reduced to avoid overheating.

Considering a particle outlet temperature of 1060 °C, and the c_p given in Table 2, the power absorbed by the material can be calculated as 9.92 kW, corresponding to a thermal efficiency of 62.1%.

The same reactor configuration is used with CRM for chemical tests. The CRM motion was studied first in cold state, showing good mixing and no dust deposition on the window. In contrast, in hot state severe deposition on the window is observed. This is due to the reaction gas which evolves directly from the bed, transporting more fine particles. Additionally, the applied suction system got clogged. The system is shown in Fig. 7, where (a) shows the condition before operation and (b) after the operation. One of the clogged suction pipes can be seen at the bottom of Fig. 7b. Since the CRM is not dried before feeding, the clogging may have been caused by the condensation of vapour inside the pipes. This in turn causes particles to stick to the pipe. A water-cooling is applied to avoid damage to the screw feeder and temperatures below 100 °C were recorded close to the suction point. Additionally, during the feeding the particles fall a short distance from the screw to the crucible, which causes the formation of a dust cloud at the back of the kiln and contributes to the clogging of the suction.

After both runs, the spectral transmissivity of the windows are analysed with the spectrophotometer Cary60 UV–Vis from Agilent Technologies. The wavelength range is 200–1000 μm and each window is measured at three points and the total result is the average of the three values. After the inert test the transmissivity is reduced by less than 5 percentage points. The decrease after the chemical test is much more severe and is about 15 times higher. This is due to the deposition of fine particles on the window. The particles absorb the radiation and eventually cause the melting of the window. This shows that although the continuous operation with inert particles in the closed configuration is possible it is not directly transferable to the treatment of reactive powders. This is also due to the fact, that during the reaction the CO_2 entrains particles from the bed. Another factor is the design of the hopper through which the particles exit the kiln. Dust clouds were clearly visible during the tests created by the falling of the particles onto the hopper or even directly into the storage. Changing the design of this part can have a big influence of the dust formation close to the window. Further improvements have to be done on the suction system to apply the closed configuration to the operation with reactive powders. The gas extraction strategy has to be improved through measures

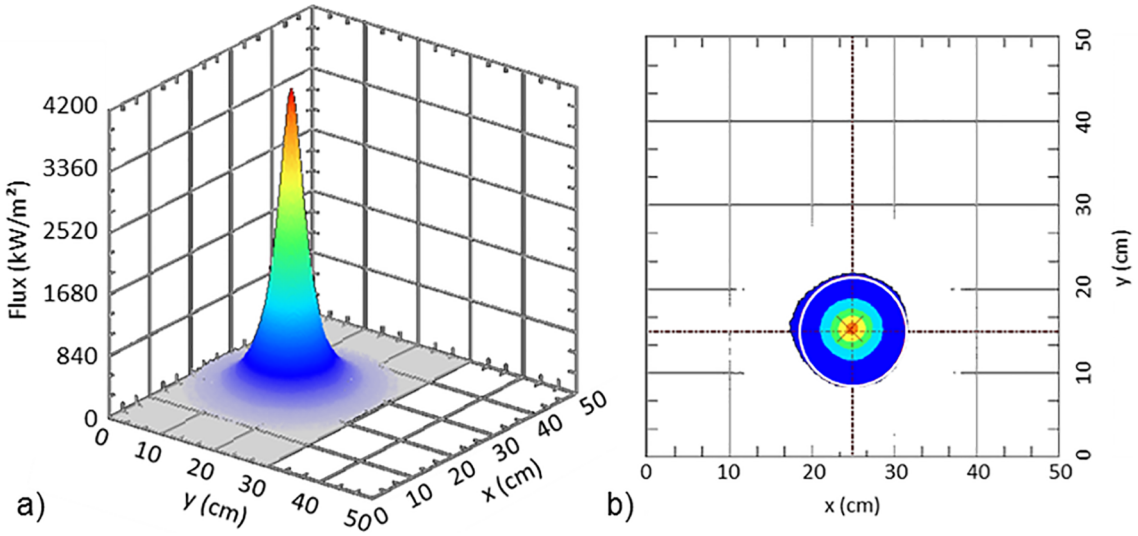

Fig. 5. Measured flux distribution (a) in 3D-view and (b) in top-view. The flux is measured at the aperture for 10 lamps. The white circle in (b) represents the aperture, where 15.96 kW of power is entering.

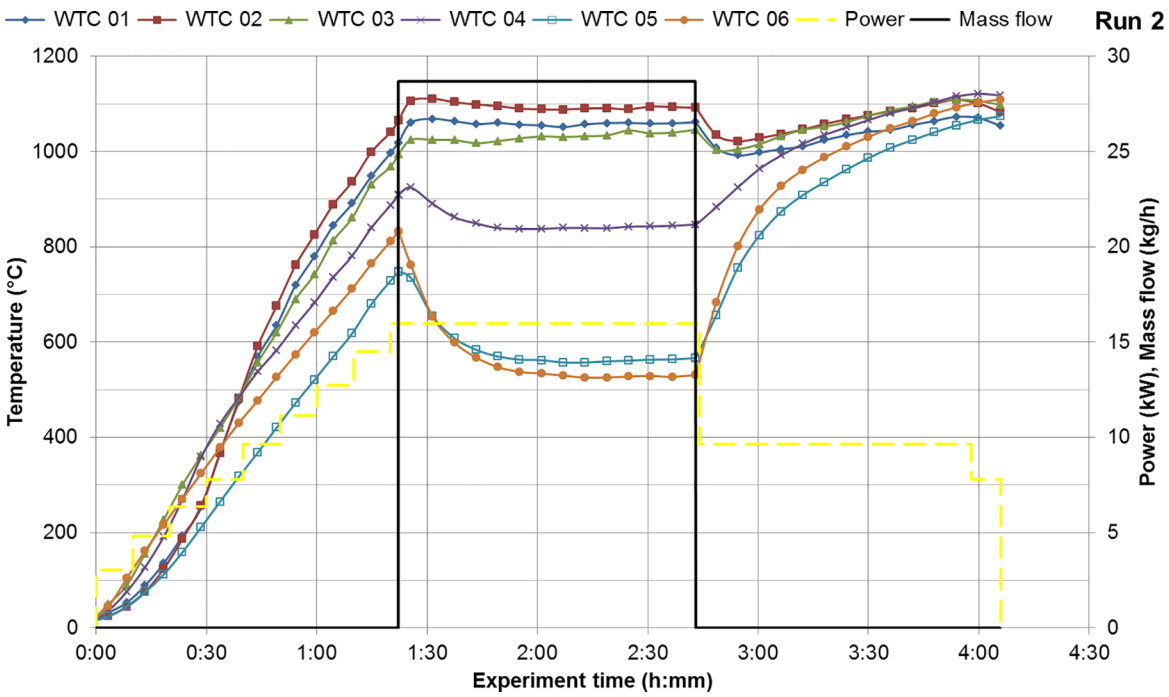

Fig. 6. Experimental run 2 performed with bauxite particles.

like an increase of the temperatures around the screw feeder to avoid condensation or by providing a short air blast to free up the suction pipes regularly.

3.2. Open configuration

The results with the closed configuration suggested analysing the calcination of CRM in the open configuration. In order to limit the amount of particles leaving the reactor and contaminating the experimental room, suctions at two points are applied (see Fig. 3b). Similar to what was reported by Meier et al. (2006) a dust cloud in the open operation of the solar rotary kiln is visible and reflecting an amount of the radiation. Nevertheless we observe the outer suction to be efficient enough to avoid contamination of the room and to allow continuous operation. Contrary to the inner suction no influence of the outer suction on the heating up of the reactor could be seen. The influence was checked by heating the reactor to a steady state without the outer suction and by turning it on afterwards. The kiln temperatures were not influenced by this. The utilized filters in the suction units were weighed before and after the whole campaign. After the chemical runs depositions in the filter are clearly visible. Nevertheless, compared to the mass of over 170 kg that was fed through the kiln during the experimental campaign, the collected amount in the filter was negligible.

The performance of the reactor is analysed in several runs with cement raw meal flow rates in the range of 4–12.4 kg/h. Remaining parameters such as the rotational speed and inclination are kept the same during these tests. The power varied slightly between 14.2 kW and 14.6 kW. Fig. 8 represents a typical test (run 5) with a particle flow of 11.4 kg/h. The heating up took 1 h longer in the open configuration compared to the closed configuration, indicating a lower thermal efficiency due to the applied suction. A temperature of 900 °C is reached at the front (WTC 01) after 2.5 h. After the start of the feeding, the front temperature (WTC 01) stabilizes at a temperature of about 890 °C, while the highest temperature of about 970 °C, obtained more inside (WTC 03). Keeping the front temperatures significantly above 900 °C is crucial to assure that the material has enough time for full calcination and avoid any recarbonation of the material. The product leaving the reactor first, when temperatures were intermittently close to 950 °C, shows a calcination of 73%. The average degree of calcination for samples collected in steady state during run 5 is only 45% leading to a chemical efficiency of 15%. In contrast, 21.7% of the incident energy is used for the heating of the material resulting in a total efficiency of 36.7%. Several runs with a material flow of 4–4.7 kg/h showed a degree of calcination of over 90%. The chemical and total efficiencies were about 12% and 21% respectively. With a flow of material of 7.7 kg/h in experimental run 8 (data given in Table 3) the outlet temperature is

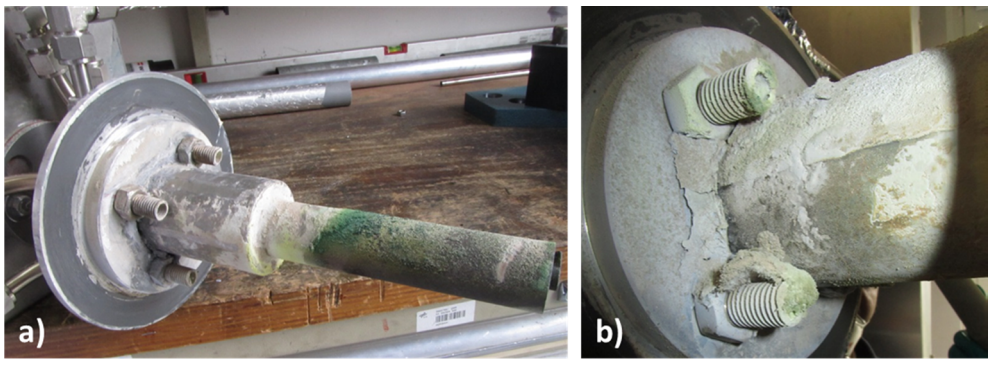

Fig. 7. Picture of the suction system (a) before and (b) after operation with CRM. After the operation, the pipe at the bottom is fully clogged.

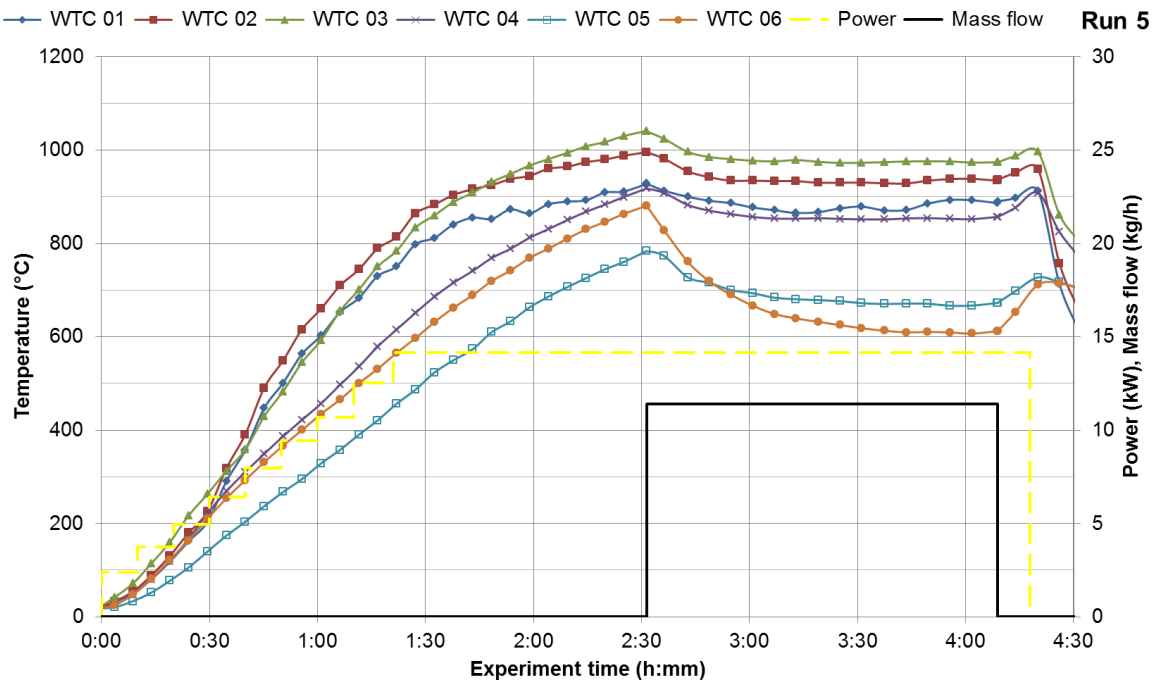

Fig. 8. Experimental run 5 performed with CRM.

always above 965 °C and an average front temperature of about 1000 °C is achieved. Unfortunately this experiment couldn't be completed due to clogging issues in the hopper 30 min after the start of the feeding. For this only samples before this point are considered. The degree of calcination in this run is for all three samples above 95%, showing very promising results for further campaigns. The chemical efficiency increased to 20.4%, while the total efficiency stayed in the same range with 37.4%.

3.3. Efficiency and influences on performance

Fig. 9a gives an overview of the achieved efficiencies during the 21 runs as a function of the particle mass flow. For the 4 tests in the closed configuration with bauxite particles the total efficiency is equal to the thermal efficiency. For the remaining 17 runs with CRM the chemical and total efficiencies are shown. With the bauxite particles an increase in mass flow resulted in an increase of reactor efficiency. Thermal efficiencies of up to 62% could be reached. Total efficiencies for the chemical runs were in the range of 19–40% and chemical efficiencies in the range of 8–20%. It can be observed how the total efficiency increases with the mass flow. Contrarily, the chemical efficiency does not show the same increase. This means although more of the incident energy is taken up by the particle bed, it is not absorbed by the reaction. The achieved degree of calcination as a function of the mass flow is shown in Fig. 9b. The results show a linear correlation and a decrease in the degree of calcination with increasing feed rates. Nevertheless, the data is much spread as can be seen for multiple runs performed with a feeding rate of about 6 kg/h and 11 kg/h. The degree of calcination varied as much as 25 percentage points for very similar feeding rates.

One reason for this could be the residence time in the kiln. Having a higher residence time would allow the reaction to proceed further and thus result in higher degrees of calcination. Comparison of the residence time in dependency on the flow rate did not show any or only a slight correlation. This finding is in agreement with those in the

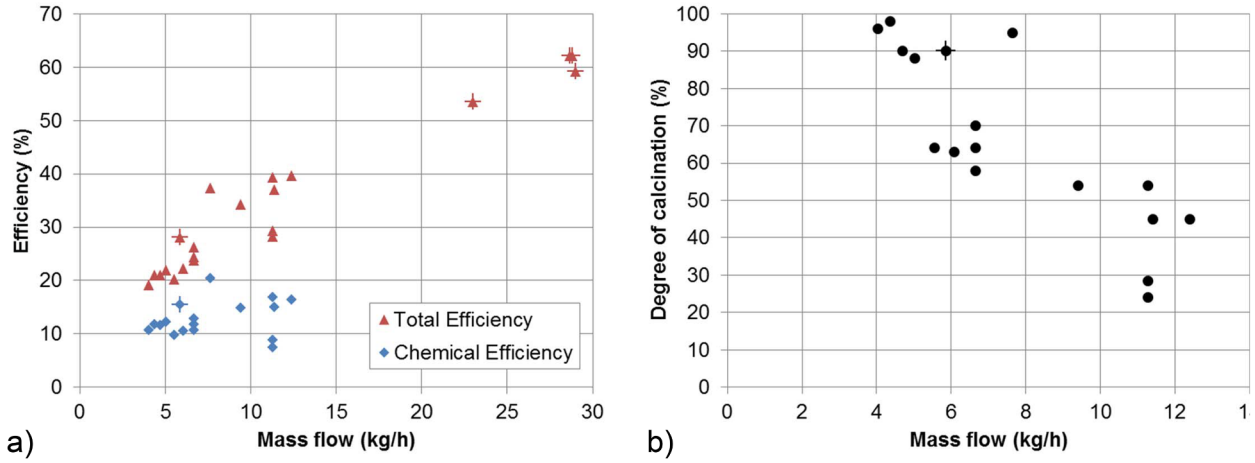

Fig. 9. (a) Overview of achieved total and chemical efficiencies for all runs. (b) Degree of calcination for the middle sample in all chemical runs. Symbols with a plus represent runs in the closed configuration whereas symbols without a plus represent runs in the open configuration.

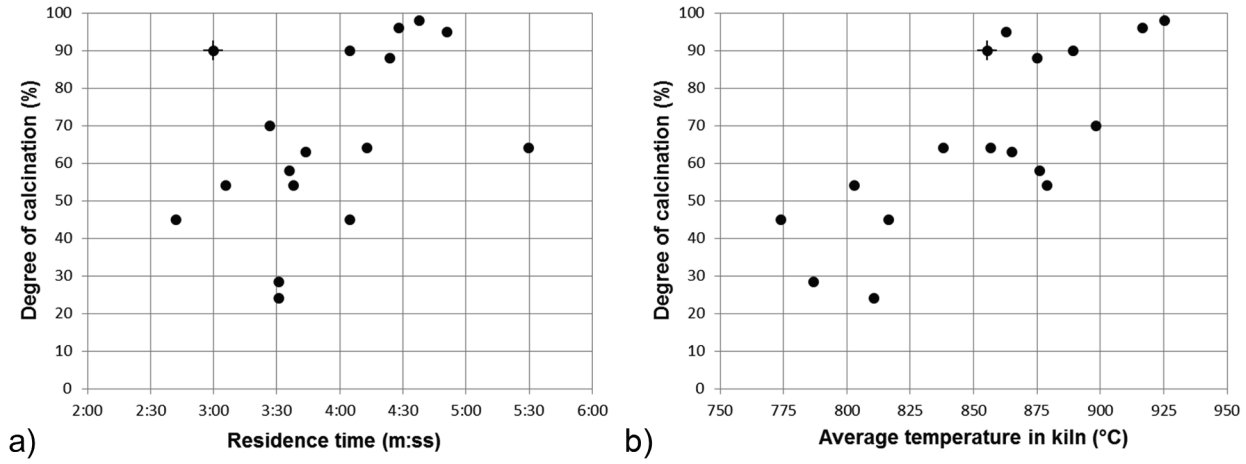

Fig. 10. Degree of calcination for the middle sample in dependency (a) on the residence time and (b) on the average kiln temperature. The symbol with a plus represents a run in the closed configuration.

literature, where a clear influence of the feeding rate could not be seen (Sullivan et al., 1927; Saeman, 1951; Liu and Specht, 2006). Similarly, the degree of calcination does not show a clear dependency on the residence time and the data is broadly distributed, as shown in Fig. 10a. Residence times of about 4 min resulted in calcination degrees as low as 45% or as high as 90%.

Another influence on the calcination is the temperature in the kiln. The dependency of the degree of calcination on the average kiln temperature is shown in Fig. 10b. Although in general higher calcinations were achieved at higher temperatures, the data is again much spread. For the same kiln temperature of 875 °C calcination degrees of 54% and 88% were achieved. However, the temperatures in the kiln had another effect on the operation. Due to sintering, the material formed layers in some positions. These layers enhanced the mixing of the bed as was visible through an IR camera. This behaviour will be further analysed in an ongoing study. The improved mixing allowed the uptake of the heat into the inner part of the bed and enhanced the calcination. Most of the runs achieved temperatures above 900 °C over half of the kiln length. Therefore, incomplete mixing of the bed is the main reason for low degrees of calcination. Temperatures above 900 °C should cause a very fast calcination of the particles, considering the very small particle size. According to kinetic studies performed by Vosteen in 1974, $CaCO_3$ particles with a size of 30 µm require less than 4 s for a full calcination at 900 °C in a CO_2-free atmosphere (Vosteen, 1974). This value increases to 6 s if the surrounding atmosphere contains 40% CO_2 and to about 12 s if the particle size increases to 100 µm. Considering that 90% of the used CRM was smaller than 100 µm and that the residence time in the kiln equalled to 210 s for most of the runs, the low calcination degrees cannot be explained only with the kinetics. The appearance of such high temperatures without a full calcination of the particle bed is therefore due to bad mixing. The outer part of the bed is heated above the reaction temperature while the core is still not fully reacted. Similar behaviour was observed by Watkinson and Brimacombe in their work on the calcination of limestone in a rotary kiln (Watkinson and Brimacombe, 1982). The effect of feed rate on axial temperature profiles in the kiln was analysed. For the highest mass flow, temperatures in the calcination zone were higher than for a lower mass flow. This again did not result in higher calcination degrees and is an indication of bad mixing.

3.4. Energy balance

To understand and further improve the operation of the rotary kiln a simple energy balancing of the reactor is done. The model separates the heat losses in four terms for the closed configuration and three terms for the open configuration:

- $\dot{Q}_{\mathrm{loss,rad}}$: Radiation losses through the aperture. Calculations were performed taking reactor temperatures and local view factors of the crucible to the aperture into account according to,

$$\dot{Q}_{\mathrm{loss,rad}} = \sigma \cdot \varepsilon_{\mathrm{crucible}} \cdot (T_i^4 - T_{\mathrm{room}}^4) \cdot F_{i,\mathrm{Apert}} \cdot A_i.$$

The view factors $F_{\mathrm{i,Apert.}}$ for the crucible and the front flange to the aperture were taken from literature (Howell, 2018). The emissivity of the crucible is taken as 1.

- $\dot{Q}_{\mathrm{loss,housing}}$: Combined convective and radiation losses for the static and rotating part of the kiln. Both parts have different temperatures and conditions due to the gas flow induced by rotation. Only the lateral surfaces are considered according to,

$$\dot{Q}_{\mathrm{loss,housing}} = A_{\mathrm{housing}} (\alpha \cdot (T_{\mathrm{housing}} - T_{\mathrm{room}}) + \sigma \cdot \varepsilon_{\mathrm{housing}} \cdot (T_{\mathrm{housing}}^4 - T_{\mathrm{room}}^4))$$

The heat transfer coefficient α for the static and rotating cylinder were taken from the VDI Heat Atlas (Kast et al., 2010; Gnielinski, 2010). The emissivity of the housing is taken as 0.05 (Kabelac and Vortmeyer, 2010).

- $\dot{Q}_{\mathrm{loss,cooling}}$: Losses due to the water cooling of the screw feeder. An energy balance of the water flow was done according to,

$$\dot{Q}_{\mathrm{loss,cooling}} = \dot{m}_{\mathrm{water}} \cdot c_p \cdot (T_{\mathrm{out}} - T_{\mathrm{in}}).$$

The water flow rate was measured experimentally.

- $\dot{Q}_{\mathrm{loss,other}}$: This value combines all unknown losses which could not be determined since at those points no temperatures or gas flows were measured. It includes losses from the front and back plate of the kiln, losses through the suctions in both configurations and convection losses through the aperture in the open configuration.

The final energy balance is thus:

$$\dot{Q}_{\mathrm{solar}} = \dot{Q}_{\mathrm{thermal}} + \dot{Q}_{\mathrm{chemical}} + \dot{Q}_{\mathrm{loss,rad}} + \dot{Q}_{\mathrm{loss,housing}} + \dot{Q}_{\mathrm{loss,cooling}} + \dot{Q}_{\mathrm{loss,other}}. \quad (4)$$

This balance is applied to all runs and the results for 8 runs will be discussed. Table 3 presents the overview of operating conditions and the results. Except for the run with the least feeding rate of 4 kg/h, the sum of the losses through the aperture, housing and cooling are similar and in the range of 18–26%. The biggest fluctuations can be seen in the amount of $\dot{Q}_{\mathrm{loss,other}}$.

Table 3
Energy balance and comparison of 8 exemplary runs (Th. = Thermal, Ch. = Chemical).

Run number	1	2	3	4	5	6	7	8
Configuration	Closed	Closed	Closed	Open	Open	Open	Open	Open
Experiment type	Th.	Th.	Ch.	Ch.	Ch.	Ch.	Ch.	Ch.
$\dot{m}$ (kg/h)	23.0	28.7	5.9	4	11.4	12.4	9.4	7.7
T_{out} (°C)	1020	1060	970	965	890	870	935	995
$\dot{Q}_{solar}$ (kW)	14.2	16.0	14.2	14.6	14.2	14.2	14.2	14.2
X_{calc} (%)	–	–	91–97	96–99	44–73	55–62	50–93	95–97
				Ratio of $\dot{Q}_{solar}$ (%)				
$\dot{Q}_{loss,rad}$	11.7	11.2	11.0	7.8	9.1	8.4	9.2	11.5
$\dot{Q}_{loss,housing}$	4.7	4.1	4.6	3.6	4.6	4.5	5.8	4.6
$\dot{Q}_{loss,cooling}$	8.5	7.4	8.5	2.1	6.9	6.9	4.6	9.7
$\dot{Q}_{loss,other}$	21.6	15.2	47.9	67.4	42.5	40.7	46.2	36.8
$\dot{Q}_{thermal}$ ($\hat{=}\eta_{th}$)	53.5	62.1	12.6	8.4	22.0	23.2	19.3	17.0
$\dot{Q}_{chemical}$ ($\hat{=}\eta_{ch}$)	–	–	15.5	10.7	15.0	16.4	14.9	20.4
$\dot{Q}_{total}$ ($\hat{=}\eta_{tot}$)	53.5	62.1	28.0	19.1	37.0	39.6	34.2	37.4

Table 4
Implications of heat recovery measures applied to run 8 and resulting total reactor efficiencies.

Heat recovered from	Total efficiency with heat recovery of			
	0%	25%	50%	75%
$\dot{Q}_{loss,cooling}$	37.4%	39.8%	42.3%	44.7%
$\dot{Q}_{loss,other}$	37.4%	46.6%	55.8%	65.0%
$\dot{Q}_{loss,cooling} + \dot{Q}_{loss,other}$	37.4%	49.0%	60.7%	72.3%

The difference can be attributed to convection losses at the aperture, through the suction system and losses due to the reflection of incident radiation caused by the dust cloud in the kiln. Calculations of convection losses show that a big part of the energy may be lost through the suction system. The temperature of the sucked off gas was in the range of 410–430 °C for the analysed chemical runs. The volumetric flow rate of the suction system was measured as 590 l/min after the experiments with the used filter. This corresponds to 4.6 kW, i.e. 32% of the incident power. This estimation is in good agreement with the additional losses due to operating without a window.

In our case the system is not optimized which leaves room for improving measures. These could be the reduction of the suction, a more locally targeted application of it or the usage of a heat exchanger to recover energy. An optimized suction system would also reduce the amount of ambient air sucked in and thus increase the concentration of CO_2 in the gas stream. Table 4 gives an idea of the implications of heat recovery measures applied to $\dot{Q}_{loss,cooling}$ and $\dot{Q}_{loss,other}$. Recovering the cooling losses has a minor impact, while recovering even 50% of the other losses would result in a total reactor efficiency of 56%. This is a clear indication that a potential upscaling will have to consider such a recovery.

4. Conclusions and outlook

Experiments with a solar rotary kiln were performed in DLR's solar simulator in Cologne, Germany. While first tests were focused on the thermal characterization of the kiln, afterwards its final use as a solar reactor for the treatment of fine particles was assessed. The goal was to show the calcination of cement raw meal with high efficiency. For this, two configurations were realised, a closed and an open one. Due to clogging issues in the suction unit continuous testing with the closed configuration was not possible. One reason was the humidity in the cement raw meal. The humidity would be drastically reduced when the solar rotary kiln is coupled to a cement plant, where drying of the meal is one of the steps before the calcination. Another reason is the severity of dust formation inside the kiln which is significantly different from cold testing, which were performed successfully. After switching to the open configuration the dust could be kept under control and succesful operation was shown in several runs. The degree of calcination for the samples in the open configuration was between 24 and 99%. Chemical efficiencies between 8 and 20% and total efficiencies between 19 and 40% were reached. Variation of the residence time did not show any clear effect on the calcination degree. On the contrary the temperature showed a clear impact. The main influence of higher temperatures was the formation of layers due to sintering which enhanced the mixing of the bed.

To determine which aspects are most promising for more efficient operation, a loss analysis was performed. One key point is the realisation of the suction unit which was shown as the biggest source of energy losses. The challenge is to have a suction system strong enough to suck off the CO_2 evolving during the reaction while keeping the amount of ambient air being sucked in at the minimum. Another possibility would be to use a closed reactor configuration to avoid these convectional losses.

The promising results obtained in this study pave the way to a potential scale up of this concept. The key to optimize the operation of such a system is to adjust parameters like the rate of suction and the mixing, which is mainly driven by rotation speed, inclination and bed height inside the kiln.

Declaration of interest

None.

Acknowledgements

This project has received funding from the European Union's Horizon 2020 research and innovation programme under grant agreement No. 654663, SOLPART project. The authors would like to thank CEMEX Research Group AG (Switzerland) for providing the material and the solar furnace team at the DLR Cologne for their support.

References

Abanades, S., André, L., 2018. Design and demonstration of a high temperature solar-heated rotary tube reactor for continuous particles calcination. Appl. Energy 212, 1310–1320.
Alonso, E., Romero, M., 2015. Review of experimental investigation on directly irradiated

particles solar reactors. Renew. Sustain. Energy Rev. 41, 53–67.
Andreotti, B., Forterre, Y., Pouliquen, O., 2013. Granular Media: Between Fluid and Solid. Cambridge University Press, Cambridge.
Dibowski, G., Neumann, A., Rietbrock, P., Willsch, C., Säck, J.-P., Funken, K.-H., 2007. Der neue Hochleistungsstrahler des DLR – Grundlagen, Technik, Anwendung. RESEARCH, D. E. V.-I. O. S., ed. 10. Kölner Sonnenkolloquium 2007, 21.06.2007. DLR e.V. – Institute of Solar Research, Köln.
Falcone, P.K., Noring, J.E., Hruby, J.M., 1985. Assessment of a Solid Particle Receiver for a High Temperature Solar Central Receiver System. Sandia National Laboratories.
Flamant, G., Hernandez, D., Bonet, C., Traverse, J.-P., 1980. Experimental aspects of the thermochemical conversion of solar energy; decarbonation of $CaCO_3$. Sol. Energy 24, 385–395.
Gnielinski, V., 2010. G6 Heat Transfer in Cross-flow Around Single Tubes, Wires, and Profiled Cylinders. VDI Heat Atlas. Springer, Berlin, Heidelberg.
Henein, H., Brimacombe, J.K., Watkinson, A.P., 1983. Experimental study of transverse bed motion in rotary kilns. Metall. Trans. B 14, 191–205.
Ho, C.K., 2016. A review of high-temperature particle receivers for concentrating solar power. Appl. Therm. Eng. 109 (Part B), 958–969.
Howell, J.R. 2018. A Catalog of Radiation Heat Transfer Configuration Factors 3rd Edition [Online]. Available: <http://www.thermalradiation.net/indexCat.html> (accessed September 27th 2018).
Imhof, A., 1991. The cyclone reactor—an atmospheric open solar reactor. Sol. Energy Mater. 24, 733–741.
Imhof, A., 1996. Decomposition of limestone in a solar reactor. Renew. Energy 9, 661–663.
Imhof, A., 1997. Decomposition of limestone in a solar reactor. Renew. Energy 10, 239–246.
Imhof, A., 2000. Calcination of limestone in a solar reactor. ZKG Int. 53, 504–509.
Imhof, A., Suter, C., Steinfeld, A., 1991. Solar thermal decomposition of $CaCO_3$ on an atmospheric open cyclone reactor. In: Proceedings of the Biennial Congress of the ISES, pp. 2091–2096.
Kabelac, S., Vortmeyer, D., 2010. K1 Radiation of Surfaces. VDI Heat Atlas. Springer, Berlin, Heidelberg.
Kast, W., Klan, H., Thess, A., 2010. F2 Heat Transfer by Free Convection: External Flows. VDI Heat Atlas. Springer, Berlin, Heidelberg.
Kohlhaas, B., Labahn, O., 1983. Cement Engineers' Handbook. Bauverlag, Wiesbaden.
Liu, X.Y., Specht, E., 2006. Mean residence time and hold-up of solids in rotary kilns. Chem. Eng. Sci. 61, 5176–5181.
Lumay, G., Boschini, F., Traina, K., Bontempi, S., Remy, J.-C., Cloots, R., Vandewalle, N., 2012. Measuring the flowing properties of powders and grains. Powder Technol. 224, 19–27.
Meier, A., Bonaldi, E., Cella, G.M., Lipinski, W., 2005. Multitube rotary kiln for the industrial solar production of lime. J. Sol. Energy Eng. 127, 386–395.
Meier, A., Bonaldi, E., Cella, G.M., Lipinski, W., Wuillemin, D., 2006. Solar chemical reactor technology for industrial production of lime. Sol. Energy 80, 1355–1362.
Meier, A., Bonaldi, E., Cella, G.M., Lipinski, W., Wuillemin, D., Palumbo, R., 2004. Design and experimental investigation of a horizontal rotary reactor for the solar thermal production of lime. Energy 29, 811–821.
Nikulshina, V., Halmann, M., Steinfeld, A., 2009. Coproduction of syngas and lime by combined $CaCO_3$-calcination and CH_4-reforming using a particle-flow reactor driven by concentrated solar radiation. Energy Fuels 23, 6207–6212.
NREL, 2018. National Renewable Energy Laboratory, U.S.A. Concentrating Solar Power Projects [Online]. Available: <https://www.nrel.gov/csp/solarpaces/> (accessed January 4th 2018).
Oates, J.A.H., 1998. Lime and Limestone: Chemistry and Technology, Production and Uses. Wiley-VCH, Weinheim; New York.
Olivier, J.G.J., Janssens-Maenhout, G., Muntean, M., Peters, J.A.H.W., 2016. Trends in Global CO2 Emissions: 2016 report.
Rhodes, M., 2008. Introduction to Particle Technology. John Wiley & Sons.
Saeman, W., 1951. Passage of Solids Through Rotary Kilns. Chem. Eng. Prog. 47.
SAINT-GOBAIN, 2013. Sintered Bauxite High Density Proppants Data Sheet. SGP-0006-DS-913-SGCS.
Sprung, S., 2008. Cement. Ullmann's Encyclopedia of Industrial Chemistry.
Steinfeld, A., Imhof, A., Mischler, D., 1992. Experimental investigation of an atmospheric-open cyclone solar reactor for solid-gas thermochemical reactions. J. Sol. Energy Eng. 114, 171–174.
Sullivan, J.D., Maier, C.G., Ralston, O.C., 1927. Passage of Solid Particles Through Rotary Cylindrical Kilns. GUS Government Printing Office.
Tescari, S., Moumin, G., Bulfin, B., De Oliveira, L., Schaefer, S., Overbeck, N., Willsch, C., Spenke, C., Thelen, M., Roeb, M. & Sattler, C. 2017. Experimental and Numerical analysis of a Solar Rotary Kiln for Continuous Treatment of Particle Material. SolarPACES 2017. Santiago, Chile.
Tregambi, C., Salatino, P., Solimene, R., Montagnaro, F., 2018a. An experimental characterization of Calcium Looping integrated with concentrated solar power. Chem. Eng. J. 331, 794–802.
Tregambi, C., Solimene, R., Montagnaro, F., Salatino, P., Marroccoli, M., Ibris, N., Telesca, A., 2018b. Solar-driven production of lime for ordinary Portland cement formulation. Sol. Energy 173, 759–768.
Vosteen, B., 1974. Vorwärmung und vollkommene Kalzination von Zementrohmehl in einem Schwebegassystem. Zement-Kalk-Gips 9, 443–450.
Watkinson, A., Brimacombe, J., 1982. Limestone calcination in a rotary kiln. Metall. Trans. B 13, 369–378.
Wicks, C.E., Block, F.E., 1963. Thermodynamic Properties of 65 Elements: Their Oxides, Halides, Carbides and Nitrides. US Government Printing Office.